Mon. Not. R. Astron. Soc. **288,** 565–571 (1997)

Kinematics of low-mass X-ray binaries and millisecond pulsars

R. Ramachandran★ and D. Bhattacharya★
Raman Research Institute, Bangalore 560080, India

Accepted 1997 January 28. Received 1996 November 18; in original form 1996 June 24

ABSTRACT

The kinematic properties of low-mass X-ray binaries and millisecond pulsars have been studied with the help of a Monte Carlo simulation. It is found that the kinematic properties of these two populations are consistent with each other, which supports the idea that LMXBs are the progenitors of millisecond pulsars. The speed distribution of millisecond pulsars is seen to be quite different from that of ordinary pulsars.

Key words: binaries: close – stars: kinematics – pulsars: general.

1 INTRODUCTION

Ever since the discovery of millisecond pulsars, they have been thought to be the products of low-mass X-ray binaries, because these systems, in which near-solar-mass donors transfer mass on to their neutron star companions (see White et al. 1995 for a review), appear to provide the ideal conditions for a neutron star to be spun up to very short periods (Alpar et al. 1982). Most, if not all, of the binary millisecond pulsars discovered in the Galactic disc have orbital characteristics and companion masses consistent with that expected of a low-mass X-ray binary (LMXB) product (Joss & Rappaport 1983; Paczyński 1983; Savonije 1983; see reviews by Bhattacharya & van den Heuvel 1991; Phinney & Kulkarni 1994; Bhattacharya 1996). However, it has been noted in the literature that a serious discrepancy in birth rate may exist between the LMXB population and the population of millisecond pulsars (Kulkarni & Narayan 1988; Coté & Pylyser 1989; Lorimer 1994, 1995), casting doubt on the origin of millisecond pulsars from LMXBs. These estimates of birth rates are still considerably uncertain, so it is important to find independent ways of testing the evolutionary link between these two classes of objects.

In this paper, we approach this issue from a kinematical point of view. If millisecond pulsars are indeed descendants of LMXBs, the spatial and velocity distributions of these two species must be compatible. If not, one may find a discernible difference between their kinematic properties. This is so because LMXBs themselves are expected to have a somewhat special velocity distribution, owing to explosive ejection of matter in the formation of the neutron stars and the attendant velocity kicks. In this work, we first try to determine what kind of intrinsic kick speed distribution may be consistent with the spatial distribution of observed LMXBs. Next, we try to infer the underlying velocity distribution of millisecond pulsars from the few measurements of transverse velocities that are available for them. Finally we compare these two results, to see whether the underlying velocity distribution responsible for generating the observed spatial distribution of LMXBs can also explain the velocity distribution of millisecond pulsars.

★E-mail: ramach@rri.ernet.in (RR); dipankar@rri.ernet.in (DB)

The exploratory work by van Paradijs & White (1995) and a more detailed population synthesis by Brandt & Podsiadlowski (1995) have attempted to determine the spatial distribution assuming a distribution of kick speeds given by Lyne & Lorimer (1993). In this work we explore a large range of kick speed distributions, in addition to the one used in the earlier papers, and also employ more detailed statistical tests. Our work shows that the Lyne & Lorimer distribution, although within acceptable limits, does not produce the best fits with the data.

The method we employ for this study is that of population synthesis via Monte Carlo simulation. We generate artificial LMXB populations based on certain initial conditions, evolutionary models and assumed kick speed distributions. The orbits of the artificial LMXBs in the Galaxy are computed, and a 'snapshot' of many such binaries at the present epoch defines the simulated population. The spatial and sky distribution of the simulated population is then compared with that of the observed LMXBs. The velocity distribution arising out of this population is compared with that of millisecond pulsars, after allowing for the fact that we are able to detect millisecond pulsars only within a small volume around the Sun.

In Section 2 we describe the assumptions and the procedure adopted in performing the Monte Carlo simulations. In Section 3 we compare the results of the simulations with observations. Section 4 contains a discussion of these results, and the conclusions drawn from them.

2 SIMULATION PROCEDURE

In our population synthesis we generate binary systems with main-sequence primary masses in the range $10 - 20\,M_\odot$ and secondaries in the range $0.2 - 1.5\,M_\odot$. The distribution of primary masses was chosen to be in accordance with the initial mass function of Scalo (1986): $\psi(M) \propto M^{-2.7}$, and the distribution of mass ratios was assumed to be uniform in the range of interest. The binary separations (a) were picked from a uniform distribution in $\log a$. The binaries then generated were evolved according to the following prescription.

2.1 Primary evolution

The primary star (M_1) overflows through its Roche lobe, transferring matter to the low-mass companion on time-scales far shorter than the thermal time-scales of the secondary. This causes spiralling in, and the orbital energy is extracted to eject the envelope of the primary. The relation between the final and initial semimajor axes is given by (Webbink 1984; Bhattacharya & van den Heuvel 1991)

$$\frac{a}{a_0} = \frac{M_2 M_{1c}}{M_{1c}+M_{1e}} \frac{1}{M_2 + 2M_{1e}/\lambda r_L}. \quad (1)$$

Here, a and a_0 are the final and initial semimajor axes respectively, M_{1c} and M_{1e} are the core and the envelope masses of the primary star respectively, $r_L a_0$ is the Roche lobe radius of the primary star, and λ is a weighting factor (< 1) for the gravitational binding energy of the core and the envelope of the star. We assume $\lambda = 0.5$ for this exercise.

We ignore the binary systems where the initial orbital energy is insufficient to expel the envelope before the secondary star merges with the helium core of the primary star. In other words, coalescing binaries are removed from our calculations. In the systems we keep, therefore, we have a low-mass main-sequence star in a close binary with a bare helium star which would eventually form a neutron star through a supernova explosion. The mass of this helium star, M_{1c}, is a function of the main-sequence primary mass M_1, and is computed using the relation of Meurs & van den Heuvel (1989): $M_{1c} = 0.415M_1 - 1.885$; M_1 and M_{1c} are in solar units.

2.2 Supernova explosions and velocity kicks

Next, we consider the supernova explosion of the helium star which leaves behind an 1.4-$M_\odot$ neutron star and ejects the remaining mass instantaneously.

Whether the binary survives the supernova explosion depends on the amount of mass lost from the system and the magnitude and the direction of the asymmetric kick velocity. The binary remains bound if (Flannery & van den Heuvel 1975; Hills 1983)

$$\Delta M \leq \frac{M_0}{2}\left[1 - \left(\frac{v_k}{v_c}\right)^2 - 2\left(\frac{v_0}{v_c}\right)\left(\frac{v_k}{v_c}\right)\cos\theta\right]. \quad (2)$$

Here, M_0 is the initial total mass of the binary system, ΔM is the amount of mass lost during the explosion, v_k is the magnitude of the asymmetric kick velocity and θ is the angle which it makes with the reduced orbital velocity v_0, and $v_c = \sqrt{GM_0/a_0}$. We retain only these surviving binaries for further consideration.

The velocity of the centre-of-mass of the binary system after the supernova explosion is given by

$$V_{cm}^2(M_{1f}+M_2)^2 = (M_{1f}v_1 - M_2 v_2)^2 + M_{1f}^2 v_k^2 + 2M_{1f}v_k(M_{1f}v_1 - M_2 V_2)\cos\theta, \quad (3)$$

where M_{1f} is the primary mass after the explosion; v_1 and v_2 are the pre-explosion orbital velocities of the two components. The final orbital semimajor axis a is computed from the initial semimajor axis a_0 using the expression (Hills 1983)

$$\frac{a}{a_0} = \left[\frac{1-(\Delta M/M_0)}{1-(2\Delta M/M_0) - Y^2}\right], \quad (4)$$

where

$$Y^2 = \left(\frac{v_k}{v_c}\right)^2 + 2\left(\frac{v_0}{v_c}\right)\left(\frac{v_k}{v_c}\right)\cos\theta.$$

Binaries that could coalesce as a result of the explosion are removed from the simulated set of objects.

2.3 Evolution of the secondary

Next, we look at the post-explosion evolution of the binary. For each of the surviving systems we choose an age (T) in the range zero to 10^{10} yr (with uniform probability) and examine whether the binary would evolve into contact during this time (although, in principle, the birth rate could be a function of time, we have chosen for simplicity a time-independent birth rate). One possible route to contact is via nuclear evolution of the secondary, when it becomes a red giant and fills its Roche lobe. If the time-scale for this to happen exceeds the assumed age of the system, then we examine the other possible route to contact, namely, angular momentum loss due to gravitational radiation and/or magnetic braking. The time-scale for the former is (Landau & Lifshitz 1975; Taylor & Weisberg 1989)

$$\tau_{GR} = 33\,701.7\, P_0^{8/3} \text{ Myr}, \quad (5)$$

where P_0 is the initial orbital period in days. The time-scale for magnetic braking is (Verbunt & Zwaan 1981; Verbunt & Hut 1983; Rappaport, Verbunt & Joss 1983)

$$\tau_{mb} = 4.35\left(\frac{M_2}{M_\odot}\right)\left(\frac{M_0}{M_\odot}\right)^{-2}\left(\frac{R_2}{R_\odot}\right)^{-\gamma}\left(\frac{a}{R_\odot}\right)^5 \text{Myr}, \quad (6)$$

where R_2 is the radius of the secondary star, a is the semimajor axis of the binary system, and M_0 is the total mass of the system. The value of γ is assumed to be 2, following Rappaport et al. (1983), who find that with this value of γ the orbital period gap in cataclysmic variables is well reproduced.

However, for magnetic braking to be effective the system must have enough time to synchronize the spin of the secondary star with the orbit. The time-scale for tidal synchronization, according to Tassoul & Tassoul (1992), is given by

$$\tau_{syn} = 5.35\times 10^{3-N/4}\left(\frac{1+q}{q}\right)\left(\frac{M}{M_\odot}\right)^{5/4} \times \left(\frac{L_\odot}{L}\right)^{1/4}\left(\frac{R_\odot}{R}\right)^3 P_0^{11/4} \text{ yr}. \quad (7)$$

Here, L, M and R are the luminosity, mass and radius of the star that undergoes tidal distortion, and q is the mass ratio of the binary system. The orbital period P_0 is in units of days. The value of the constant N, which depends on the nature of the envelope of the star, is assumed to be 6. The value of N is zero for radiative envelopes and 10 for convective envelopes. With $N \approx 6-10$, the theory of Tassoul & Tassoul (1992) provides the general trend of the data. Then, the luminosity and the radius of stars are computed from the evolutionary models of Schaller et al. (1992).

If either τ_{GR} or the larger between τ_{mb} and τ_{syn} is less than the assumed age, we regard the binary as having evolved into contact. We exclude from further computation the objects that do not evolve into contact and hence do not become LMXBs.

2.4 Motion in the Galaxy

We choose a Galactic position for each surviving binary in our sample. In the cylindrical galactocentric (R, ϕ, z) coordinates, the spatial distribution that we choose is assumed to be uniform in ϕ, Gaussian in z with a width of 75 pc (similar to the scaleheight of massive stars), and uniform in R between zero and 15 kpc (R-distributions of various kinds were later produced from this parent distribution by applying statistical weights depending on the

Table 1. Parameters of the Galactic potential model (Kuijken & Gilmore 1989).

Parameter	disc–halo	nucleus	bulge
Mass ($M_\odot$)	1.45×10^{11}	9.3×10^{11}	1×10^{10}
β_1	0.4		
β_2	0.5		
β_3	0.1		
h_1	0.325		
h_2	0.090		
h_3	0.125		
a	2.4		
b	5.5	0.25	1.5

initial R value; see Section 3). We compute the Galactic rotation speed ($V_{\rm rot}$) at the chosen position and add vectorially the centre-of-mass velocity resulting from the above expression to get the net velocity ($\boldsymbol{V}_{\rm tot}$) of the binary. The direction of $V_{\rm cm}$ with respect to the Galactic rotation is assumed to be random.

Starting with the assumed initial position and $\boldsymbol{V}_{\rm tot}$ we compute the trajectory of a binary in the Galaxy for its assumed age T. The gravitational potential that we used for these dynamical calculations is given by (Kuijken & Gilmore 1989)

$$\Phi(R,z) = \frac{-M}{\left[\left(a+\sqrt{z^2+h^2}\right)^2+b^2+R^2\right]^{1/2}}, \quad (8)$$

where R and z are the galactocentric cylindrical polar coordinates. This potential has three components, namely (i) the disc–halo, (ii) the central bulge, (iii) the nucleus. The values of the constants are listed in Table 1. For the disc–halo component $\sqrt{z^2+h^2}$ must be replaced by $\sum_{i=1}^{3}\beta_i\sqrt{z^2+h_i^2}$.

Caldwell & Ostriker (1981) discuss extensively the effect of errors in the observational constraints on the derived three-dimensional potential function of the Galaxy. Some of the main observational constraints are Oort's constants, the local surface density, the radius of the central bulge, the rotation curve of the Galaxy and the tangent points inside the solar circle. As Caldwell & Ostriker describe, changing the values of all the constraints by 1σ changes the fitted parameters of the potential by only a few per cent. Therefore we assume that the possible refinement of the Galactic potential model in the future will not change the trajectories considerably.

In computing the orbit, we ensure the conservation of orbital energy to better than one part in 10^7 using an adaptive Runge–Kutta integration scheme. The potential in equation (8) was also used to derive the Galactic rotation speed $V_{\rm rot}$ at any given R. For each such object the orbital parameters of the binary, along with the initial and final positions and velocities, are stored.

2.5 Kick speed distributions

As mentioned above, the velocity of the binary system and hence its final position depend on the asymmetric velocity kick ($v_{\rm k}$) received at the supernova explosion. There is not yet any consensus about the distribution of the kick speeds that neutron stars receive at birth. We have therefore chosen to explore several different kinds of kick speed distributions, repeating the full population synthesis for each assumed kick speed distribution. Our choice included Maxwellian distributions: $\psi(v_{\rm k}) \propto v_{\rm k}^2\exp\left(v_{\rm k}^2/2\sigma_{\rm k}^2\right)$, with $\sigma_{\rm k}$ =50, 100, 150, 200, 300 and 500 km s^{-1}, the distribution proposed by Paczyński (1990): $\psi(v) \propto 1/\left[1+(v/v_\star)^2\right]^2$ with $v_\star = 450\,{\rm km\,s^{-1}}$, and a modified version of it due to Hansen & Phinney (1996) which changes $v_\star$ to 600 km s^{-1} [we shall refer to this as the Hansen–Phinney–Paczyński (HPP) distribution in the rest of the paper]. In addition, we used the speed distribution proposed by Lyne & Lorimer (1993) (hereafter LL distribution), which we modelled based on tabulated values of the distribution function kindly supplied to us by D. R. Lorimer. For the purpose of comparison we also repeated the synthesis assuming completely spherical mass ejection in the supernova (which implies $v_{\rm k} = 0$).

3 COMPARISON WITH OBSERVATIONS

3.1 Low-mass X-ray binaries

The kinematic properties of a population of objects include their velocity distribution and their spatial distribution in the Galaxy, which are closely interrelated. Measurement of radial velocities of a few LMXBs has been reported in the literature (Cowley et al. 1987). However, the derivation of the systemic velocities of these binaries from the measured radial velocities remains notoriously difficult, and the values derived by different authors disagree by substantial amounts (Cowley et al. 1988; Augusteijn et al. 1996). We shall, therefore, refrain from using the reported radial velocities to describe LMXB kinematics, but will report at the end the dispersion of radial velocities expected from our work, with which observations can be compared once reliable measurements of radial velocities become available.

Since LMXBs are visible at large distances, their spatial distribution is much more well determined. To compare the kinematic properties of our simulated sample with observed LMXBs, we have therefore decided to use their distribution in the plane of the sky (distribution in Galactic latitude and longitude). We have also compared the results of our simulations with the distribution of the heights from the Galactic plane (z) and the projected galactocentric distance (R) of the known LMXBs for which the distance estimates exist (van Paradijs & White 1995).

The sample of real LMXBs with which we have chosen to compare our simulations is the one given by van Paradijs & White (1995). This list contains 64 sources with confirmed neutron star companions; out of these we use 60 sources which have X-ray fluxes above 10 μJy. The distribution of these sources in the Galactic coordinates is shown in Fig. 1. This flux-limited sample set is of course not entirely unbiased in terms of their distribution in the Galaxy: van Paradijs & White (1995) find that a larger fraction of them are on the nearer side of the Galactic Centre than on the farther side. To account for this we assigned a detection probability of the form e^{-d/d_0} with $d_0 = 8.5$ kpc to the members of the simulated sample. However, the effect of this weighting function on the final results is seen to be less than 1–2 per cent.

The observed spatial distribution of LMXBs is influenced not only by their velocity distribution, but also by the Galactic distribution of their birth rate. One has no a priori knowledge of how the birth rate of LMXBs depends on the galactocentric radius R. In comparing our simulations with observations we have kept the birth rate distribution variable: we assume the distribution to be composed of two components, (i) a uniform distribution in the disc, and (ii) a Gaussian centred at the Galactic Centre. The relative weight w of these two components and the width R_0 of the Gaussian component are kept variable. For every assumed kick speed distribution we determine the combination of w and R_0 that produces the best possible match between the Galactic latitude

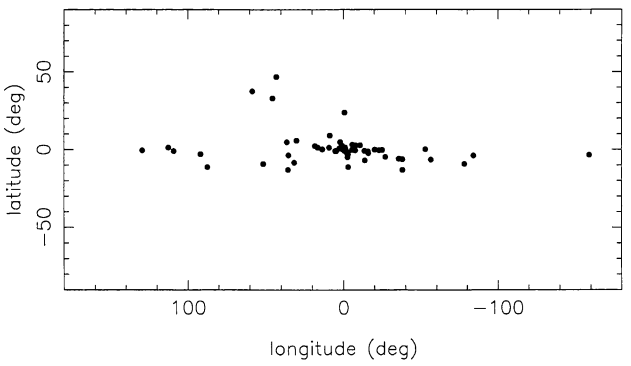

Figure 1. The distribution of LMXBs in Galactic coordinates. Only the LMXBs with confirmed neutron star companions are plotted here (see van Paradijs & White 1995).

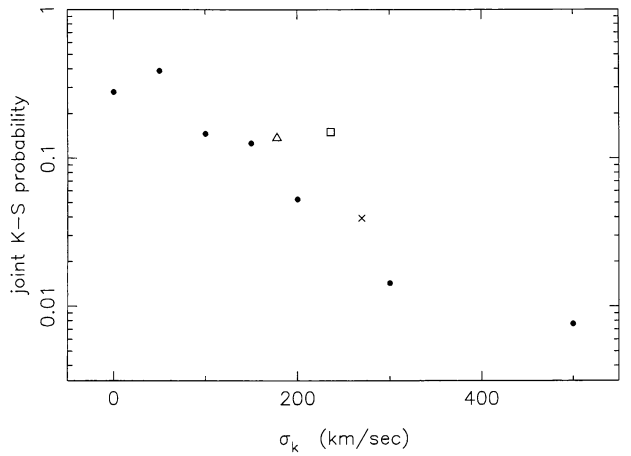

Figure 2. The distribution of maximum joint KS probabilities for LMXBs as a function of σ_k. The dots indicate Maxwellian kick speed distributions of σ_k = zero, 50, 100, 150, 200, 300 and 500 km s^{-1} (the root mean square speed of a Maxwellian distribution is $\sqrt{3}\times\sigma_k$). The LL, Paczyński and HPP distributions are indicated by the cross, triangle and square, with average speeds of 430, 284 and 376 km s^{-1}, respectively. For these three distributions, the x-axis value indicates $\sqrt{\pi/8}$ times the average speed.

and longitude distributions of the simulated and the observed LMXBs. As it turns out, the values of w and R_0 that produce the best matches are nearly the same for all assumed kick speed distributions, with the width of the Gaussian component $\sim$ 0.8 kpc, and the ratio of the net birth rate in the uniform component to that in the Gaussian component of $\sim$1.9. Generation of populations corresponding to many different radial birth rate distributions is made possible by using statistical weights. Every object is assigned a weight proportional to the probability of birth at its *initial* position in R. By varying these R-dependent weights one could simulate any intrinsic birth rate distribution. For computations following this stage, we freeze these weights corresponding to the best-match birth rate distribution [corresponding to the highest joint Kolmogorov–Smirnov (KS) probability for the distribution of l and b] for the respective kick speed distribution. A comparison of such best fits for different kick speed distributions is shown in Fig. 2. As can be seen, Maxwellians with characteristic velocities $\leq$150 km s^{-1}, and the HPP as well as the Paczyński distributions yield some of the best-fitting probabilities.

The sample of van Paradijs & White (1995) contains 18 LMXBs for which distance estimates are available. For these sources we can compare the distribution of z and R with that of our simulated sample. Interestingly, the joint KS probability in this case follows exactly the same trend as derived from the sky distribution, although the formal statistical significance of the latter result is poorer because of a much smaller observed sample.

3.2 Millisecond pulsars

Unlike LMXBs, the population of known millisecond pulsars is strongly biased by observational selection effects. Most millisecond pulsars we know are located very close to the Sun, and we have practically no knowledge of the large-scale distribution of millisecond pulsars in the Galaxy. As a result, the spatial distribution of known millisecond pulsars cannot be used to compare with that of LMXBs or even that of our simulated population. However, measurements of transverse velocities are available for several millisecond pulsars. So in this case we compare the transverse velocity distribution of the simulated sample with that of the observed sample.

Since the observed number of millisecond pulsars in the Galactic disc is small, we have not attempted a detailed modelling of selection effects as is usually done in similar studies of normal pulsars (Narayan 1987; Narayan & Ostriker 1990). Instead, we note that almost all known millisecond pulsars are located in a region ζ bounded by, in galactocentric cylindrical coordinates, $7.2 \leq R(\mathrm{kpc}) \leq 9$, $|z| \leq 1$ kpc, and $|\phi| \leq 12^\circ$ around the location of the Sun (see Fig. 3). Out of 12 pulsars for which velocity measurements are available, 10 fall within this range. These pulsars are listed in Table 2. We compare the transverse velocity distribution defined by these 10 pulsars with that of the simulated objects falling within the above boundary. The transverse velocities of the simulated objects are calculated as follows. From the final velocity of each simulated object, the Galactic rotation velocity corresponding to its location is removed, i.e., the peculiar velocity of each object is computed in its local standard of rest. Then, the transverse velocity of each object is computed by taking the projection of the peculiar velocity perpendicular to the line joining the Sun and the object. For a known millisecond pulsar the distance is computed from the dispersion measure using the electron density distribution model of Taylor & Cordes (1993). The transverse velocity of the pulsar is then computed after removing the solar peculiar motion, and differential Galactic rotation between the Sun and the location of the pulsar. These values are listed in Table 2.

As noted by Nicastro & Johnston (1995), the restriction of the observable volume of millisecond pulsars to within a small volume around the Sun (as in Fig. 3) might cause the observed transverse velocity distribution to be deficient in high velocities. Fig. 4 shows the distribution of centre-of-mass speeds just after the primary star explosion in binaries considered for the simulation. Fig. 5 shows the distribution of peculiar speeds after imposing the volume restriction, after evolving in the Galactic gravitational potential for ages up to 10 Gyr. It can be seen that the distributions in Fig. 5 are narrower than the corresponding distributions in Fig. 4. The reason for this is twofold: the evolution in the Galactic potential for long time-scales like 10 Gyr modifies the input speed distributions significantly, and a significant fraction of high-speed objects escape from the observable volume. However, one must keep in mind that a fraction of the population of objects escaping from the observable volume become replenished by the objects drifting out from the inner portions of the Galaxy. We now perform a

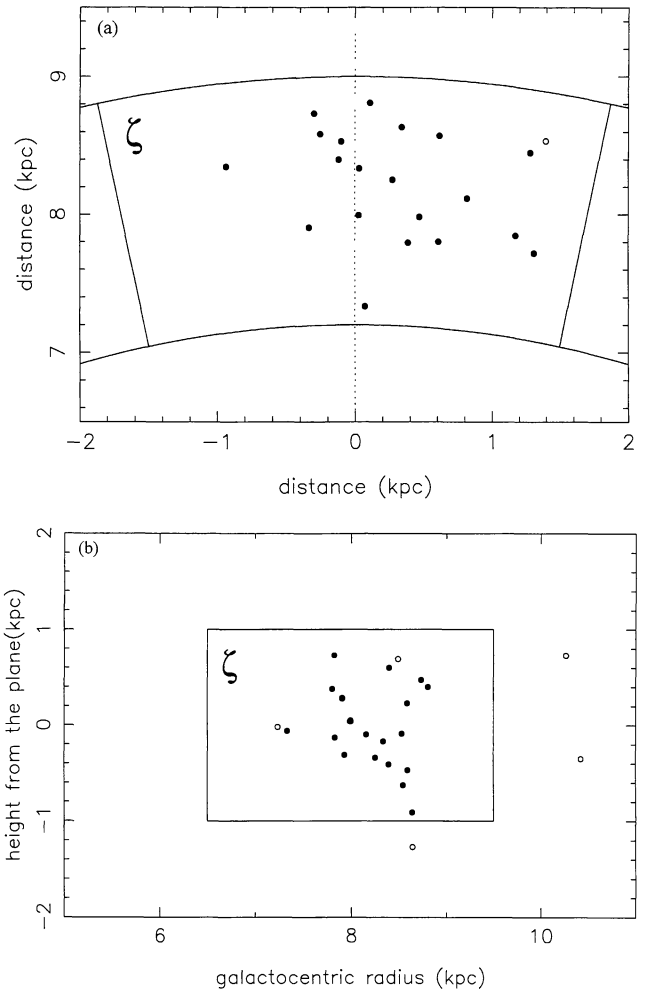

Figure 3. The distribution of millisecond pulsars in the Galaxy. (a) Distribution in the Galactic plane, where the Galactic Centre is at the origin (0, 0), and the Sun is at (0, 8.5). Two arcs are drawn with galactocentric radii of 7.2 and 9 kpc respectively. Two lines are drawn with azimuth angles [defined in the conventional sense of $\tan^{-1}(Y/X)$] of 78° and 102°. (b) The distribution as a function of the galactocentric radius and the height from the Galactic plane (z). The box drawn has limits in z of ± 1 kpc, and in R of 7.2 and 9 kpc. Pulsars that fall within this range (indicated by ζ) are indicated by filled circles. See Section 3.2 for details.

comparison of the distribution of the Galactic rotation corrected transverse velocities of 10 millisecond pulsars with that of the simulated population by means of a KS test. The results of these tests are shown in Fig. 6. As the number of observed objects is very small, this test is of limited usefulness, but we consider the relative comparison of KS probabilities to be a rough indicator of the merit of different kick speed distributions. Fig. 6 suggests that Maxwellian distributions of $\sigma_k \leq 200$ km s^{-1} and the LL, Paczyński and HPP distributions all produce KS probabilities at roughly similar levels, and could be considered consistent with observations. Maxwellians of $\sigma_k \geq 300$ km s^{-1} appear to be inadmissible by the data.

The same conclusion can be arrived at by performing a somewhat different test as shown in Fig. 7. Here, we compute the first moment (mean) of the transverse velocities of 10 objects randomly picked from the simulated distribution from the region ζ. For each assumed kick velocity distribution this selection is repeated a large number of times and a distribution of the averages so computed is obtained.

Table 2. The list of millisecond pulsars with proper motion measurements. The second and third columns give the proper motions in right ascension and declination, respectively. The fourth column gives the transverse velocity after correcting for the Galactic systematic differential motion and the solar peculiar motion. The transverse velocities of the last three pulsars are from scintillation measurements. References: (1) Kaspi, Taylor & Ryba (1994), (2) Arzoumanian, Fruchter & Taylor (1994), (3) Nice & Taylor (1995), (4) Wolszczan (1994), (5) Camilo, Foster & Wolszczan (1994), (6) Bell et al. (1995), (7) Nicastro & Johnston (1995).

Name	μ_α mas/yr	μ_δ mas/yr	v km s^{-1}	Ref.
J1857+0943	−2.94	−5.41	14.9	1
J1959+2048	−16.0	−25.8	193.2	2
J2019+2425	−9.9	−21.1	84.6	3
J1300+1240	46.4	−82.9	290.7	4
J1713+0747	4.9	−4.1	27.5	5
J2322+2057	−16	−18	81.2	3
J0437−4715	114	−72	92.6	6
J1730−2304	–	–	22	7
J2145−0750	–	–	31	7
J1455−3330	–	–	60	7

Fig. 7 shows the mean and the rms values of these averages for every kick speed distribution. It can be seen that Maxwellians in the range 100–200 km s^{-1}, LL, Paczyński and HPP distributions closely reproduce the average of the observed sample.

4 DISCUSSION AND CONCLUSIONS

In this paper we have made a comparative study of the kinematic properties of LMXBs and millisecond pulsars to test the hypothesis that the latter are the evolutionary products of the former. In the case of LMXBs we have compared the sky and the spatial distribution of our synthesized population with that of the observed sample, while in the case of millisecond pulsars the comparison between the simulated and the observed samples has been made on the basis of transverse speeds. A comparison of Figs 2 and 6 reveals a remarkable similarity between the fit qualities of the synthesized and observed populations of LMXBs and millisecond pulsars, as a function of the assumed kick speed distributions. This is consistent with the idea that both classes of objects are likely to be drawn from the same parent population. In other words, within the observational uncertainties the kinematic properties of LMXBs and millisecond pulsars are consistent with each other, lending credence to the hypothesis that LMXBs are the progenitors of millisecond pulsars.

The speed distribution of LMXBs and hence millisecond pulsars may be quite different from the assumed kick speed distributions, since the speed at birth (which is the centre-of-mass speed of the binary after the supernova explosion) depends on the orbital parameters, in addition to the direction and magnitude of the kick velocity. Fig. 4 gives the distribution of centre-of-mass speeds of binaries just after the supernova explosion of the primary star. As one can see, there is a considerable difference between the kick speed distributions and the corresponding centre-of-mass speed distributions. The reason for this is twofold: if the magnitude of the asymmetric kicks is very low, then the systematic velocity after the supernova explosion is determined mainly by the mass ejected by

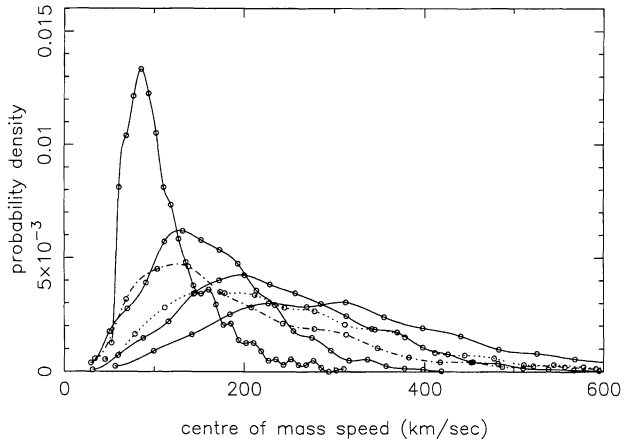

Figure 4. Centre-of-mass speed distributions corresponding to various kick speed distributions. Solid lines indicate the distributions corresponding to the input Maxwellian kick speed distributions with σ_k = zero, 100, 200 and 300 km s^{-1} (from the narrowest to the broadest). The dotted and dot-dashed lines indicate the distributions for LL and HPP, respectively.

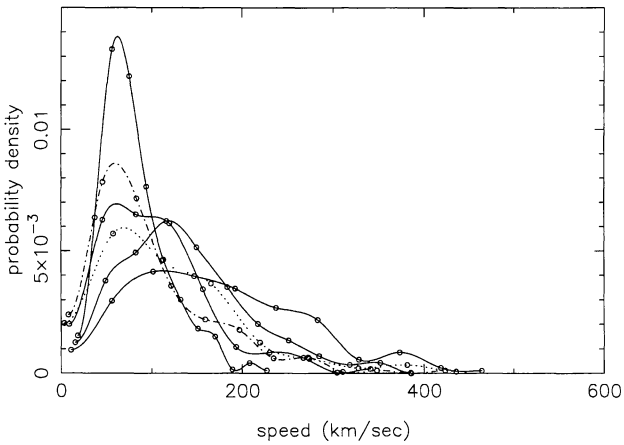

Figure 5. The speed distribution of LMXBs after imposing the volume restriction. The solid lines indicate the distributions corresponding to the input Maxwellian kick speed distributions with σ_k = zero, 100, 200 and 300 km s^{-1} (from the narrowest to the broadest). The dotted and dot-dashed lines indicate the distributions for LL and HPP, respectively.

the system, and this appears to peak around 70 km s^{-1} for the distribution of binary parameters that we have used. On the other hand, if the asymmetric kick velocities are very large (say, 300 km s^{-1}), then many systems are disrupted, the probability of remaining bound decreasing significantly. This suggests that the intrinsic velocity distribution of millisecond pulsars is significantly different from that observed for normal pulsars, which has been found to have a mean of around 400 km s^{-1} (Lyne & Lorimer 1993; Hansen & Phinney 1996).

Another possible way to discriminate between different intrinsic speed distributions would be the local birth rate implied for millisecond pulsars by these different velocity distributions. If the intrinsic velocity distribution were wider, the local birth rate needed to match with the observed number would be higher, because only a smaller fraction will remain within the observable volume. In the various kick speed distributions investigated by us, the implied local birth rate changes by a factor of 3 as we go from no asymmetric kicks to the velocity distribution of Lyne & Lorimer

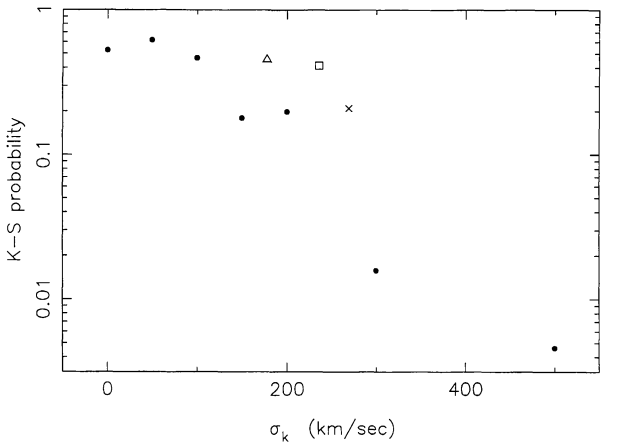

Figure 6. The distribution of maximum KS probabilities for millisecond pulsars as a function of σ_k. The dots indicate Maxwellian kick speed distributions of σ_k =zero, 50, 100, 150, 200, 300 and 500 km s^{-1}. The LL, Paczyński and HPP distributions are represented with the cross, triangle and square, with average speeds of 430, 284 and 376 km s^{-1}, respectively. For these three distributions, the x-axis values indicate $\sqrt{\pi/8}$ times the average.

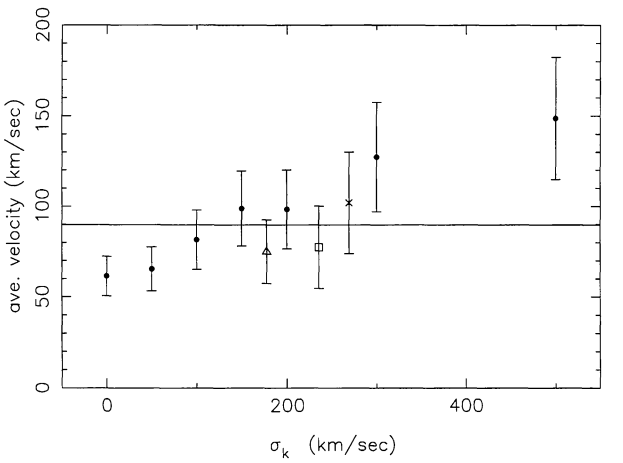

Figure 7. The results of the 'random pick' method. The horizontal solid line at 89.8 km s^{-1} is the average transverse velocity of the known millisecond pulsars. The dots indicate the mean of the distribution of averages of randomly picked set of points, as a function of σ_k. The error bar indicates the 1σ deviation of the distribution of averages. The LL, Paczyński and HPP distributions are represented by the cross, triangle and square. For these three distributions the x-axis values indicate $\sqrt{\pi/8}$ times the average value.

(1993). A detailed investigation of this is beyond the scope of the paper and will be addressed in a future communication.

From the simulated speed distribution one can try to deduce the radial velocity distribution of LMXBs. Table 3 lists the radial velocity dispersion as a function of σ_k. The second column gives the radial velocity dispersion as observed from the Sun, and the third column gives the dispersion of the radial component of the LMXB peculiar velocities (in their standard of rest). As one can see, the change in the second column is only about 50 per cent, while going from the case with no kick speed to the case with a Maxwellian kick speed distribution of σ_k = 500 km s^{-1}. This is because the dispersion is dominated by the contribution from the Galactic differential rotation.

Table 3. LMXB radial velocity dispersion for various assumed kick speed distributions.The second column gives the radial velocity dispersion observed from the Sun, and the third column gives the dispersion of the radial component of LMXB speeds in their local standard of rest.

$\sigma_{\mathbf{k}}$ (km s^{-1})	σ_{v_r} (km s^{-1})	σ_{v_r} (km s^{-1})
zero	114	64
50	117	72
100	125	87
150	128	104
200	134	112
300	139	133
500	165	155
Lyne & Lorimer	131	106
HPP	125	94
Paczyński	122	89

The main results of this paper can be summarized as follows.

(i) The kinematic properties of low-mass X-ray binaries and millisecond pulsars are consistent with each other, supporting the idea that low-mass X-ray binaries are the progenitors of millisecond pulsars.

(ii) The spatial distribution of known low-mass X-ray binaries and the measured proper motion of millisecond pulsars are consistent with kick speed distributions that allow for a significant fraction of low-speed objects. However, with the present limited sample, the distribution given by Lyne & Lorimer (1993) cannot be ruled out.

(iii) The average speeds of millisecond pulsars may be considerably less than the average speeds of normal pulsars.

ACKNOWLEDGMENT

We would like to thank V. Radhakrishnan and the referee Jan van Paradijs, for their suggestions which have helped us a great deal to improve the manuscript.

REFERENCES

Alpar M. A., Cheng A. F., Ruderman M. A., Shaham J., 1982, Nat, 300, 728
Arzoumanian Z., Fruchter A. S., Taylor J. H., 1994, ApJ, 426, L85
Augusteijn T., van der Hooft F., de Jong J. A., van Kerkwijk M. H., van Paradijs J., 1996, A&A, submitted
Bell J. F., Bailes M., Manchester R. N., Weisberg J. M., Lyne A. G., 1995, ApJ, 440, L81
Bhattacharya D., 1996, in van Paradijs J., van den Heuvel E. P. J., Kuulkers E., eds, Proc. IAU Symp. 165, Compact Stars in Binaries. Kluwer, Dordrecht, p. 243
Bhattacharya D., van den Heuvel E. P. J., 1991, Phys. Rep., 203, 1
Brandt N., Podsiadlowski P., 1995, MNRAS, 274, 461
Caldwell J. A. R., Ostriker J. P., 1981, ApJ, 251, 61
Camilo F., Foster R. S., Wolszczan A., 1994, ApJ, 437, L39
Coté J., Pylyser E. H. P., 1989, A&A, 218, 131
Cowley A. P., Hutchings J. B., Crampton D., Hartwick F. D. A., 1987, ApJ, 320, 296
Cowley A. P., Hutchings J. B., Crampton D., 1988, ApJ, 333, 906
Flannery B. P., van den Heuvel E. P. J., 1975, A&A, 39, 61
Hansen B. M. S., Phinney E. S., 1996, ApJ, submitted
Hills J. G., 1983, ApJ, 267, 322
Joss P. C., Rappaport S. A., 1983, Nat, 304, 419
Kaspi V. M., Taylor J. H., Ryba M., 1994, ApJ, 428, 713
Kuijken K., Gilmore G., 1989, MNRAS, 239, 571
Kulkarni S. R., Narayan R., 1988, ApJ, 335, 755
Landau L. D., Lifshitz E. M., 1975, The Classical Theory of Fields. Pergamon Press, Oxford
Lorimer D. R., 1994, PhD thesis, University of Manchester
Lorimer D. R., 1995, MNRAS, 274, 300
Lyne A. G., Lorimer D. R., 1993, Nat, 369, 127
Meurs E. J. A., van den Heuvel E. P. J., 1989, A&A, 226, 88
Narayan R., 1987, ApJ, 319, 162
Narayan R., Ostriker J. P., 1990, ApJ, 352, 222
Nicastro L., Johnston S., 1995, MNRAS, 273, 122
Nice D. J., Taylor J. H., 1995, ApJ, 441, 429
Paczyński B., 1983, Nat, 304, 421
Paczyński B., 1990, ApJ, 348, 485
Phinney E. S., Kulkarni S. R., 1994, ARA&A, 32, 591
Rappaport S., Verbunt F., Joss P. C., 1983, ApJ, 275, 713
Savonije G. J., 1983, Nat, 304, 422
Scalo J. M., 1986, Fundam. Cosmic Phys., 11, 1
Schaller G., Schaerer D., Meynet G., Maeder A., 1992, A&AS, 96, 269
Tassoul J., Tassoul M., 1992, ApJ, 395, 259
Taylor J. H., Cordes J. M., 1993, ApJ, 411, 674
Taylor J. H., Weisberg J. M., 1989, ApJ, 345, 434
van Paradijs J., White N., 1995, ApJ, 447, L33
Verbunt F., Hut P., 1983, A&A, 127, 161
Verbunt F., Zwaan C., 1981, A&A, 100, L7
Webbink R. F., 1984, ApJ, 277, 355
White N. E., Nagase F., Parmar A. N., 1995, in Lewin W. H. G., van Paradijs J., van den Heuvel E. P. J., eds, X-Ray Binaries. Cambridge Univ. Press, Cambridge, p. 1
Wolszczan A., 1994, Sci, 264, 538

This paper has been typeset from a TEX/LATEX file prepared by the author.